Electrocoagulation of Silica Nanoparticles in Wafer Polishing Wastewater by a Multichannel Flow Reactor: A Kinetic Study

Walter Den[1] and Chihpin Huang[2]

Abstract: A simplistic and systematic procedure has been developed for the design and upscaling of a multichannel, continuous-flow electrocoagulation reactor of monopolar configuration for the removal of submicron particles from wastewater. Using wastewater generated from the chemical-mechanical planarization process as the target wastewater, a series of laboratory-scale studies were conducted to determine the required operating conditions for the efficient removal of the ultrafine silica particles. These operating criteria included charge loading (≥ 8 F/m^3), current density (≥ 5.7 A/m^2), hydraulic retention time (≥ 60 min), as well as the initial pH (7–10). Furthermore, a steady-state transport equation with second-order reaction kinetics was employed to describe the rate of coagulation as the rate-limiting factor. The actual kinetic constant determined from the laboratory-scale experiments was approximately 1.2×10^{-21} m^3/s, which was three orders of magnitude smaller than that calculated based on Brownian coagulation. The model was subsequently validated with a series of experiments using a pilot-scale electrocoagulation reactor geometrically similar to the laboratory-scale reactor with nearly 20 times volumetric scaleup.

DOI: 10.1061/(ASCE)0733-9372(2006)132:12(1651)

CE Database subject headings: Wastewater management; Water treatment; Silica; Colloids; Kinetics; Coagulation; Laminar flow; Channel flow.

Introduction

Electrocoagulation, constituting either as an entirety or as a part of electrochemical processes, has been investigated as a treatment technology for a variety of wastewaters containing finely dispersed particles without chemical additions (Dobolyi 1978; Lin and Chi 1994; Chen et al. 2000; Tsouris et al. 2001; Holt et al. 2002; Ge et al. 2004). For electrocoagulation, the sacrificial anodic electrodes, typically made of iron and aluminum, are used to continuously supply metallic ions as the source of coagulants. These electrochemically generated metallic ions can hydrolyze near the anodic surface to form a series of metallic hydroxides capable of destabilizing dispersed particles. The simultaneous electrophoretic migration of the negatively charged particles toward the anode forces chemical coagulation between particles and metallic hydroxides in the vicinity of the anode, forming flocs that either settle or redeposit onto the anode.

One of the most notable wastewaters containing highly charged ultrafine particles is generated from the chemical-mechanical planarization (CMP), an integral process for the state-of-the-art fabrication of multilevel design of integrated circuits. The process is primarily used for "polishing" the device side of a semiconductor wafer through the mechanical downforce of slurry abrasive in combination with the chemical oxidation of wafer surface. CMP effluents typically contain suspended solids originated from slurry abrasive particles of SiO_2, Al_2O_3, or CeO_2, depending on the nature of the CMP application. Other contaminants, including insoluble metal oxides and nitrides and soluble chemicals, also exist in the wastewater in much lesser quantities. In principal, CMP wastewater contains very dilute slurry abrasives that are narrowly ranged between 50 and 200 nm, and possess highly negative surface charges that repel adjacent particles when they are immersed in base solutions (Golden et al. 2000). These wastewater characteristics render conventional coagulation and flocculation technology less ideal to remove these submicron particles from the CMP wastewater due to problems associated with overdosing and poor settling characteristics of the flocs. Among other treatment alternatives (e.g., membrane filtration), electrocoagulation has attracted much attention as an effective method for particle separation (Belongia et al. 1999; Lai and Lin 2003; Den and Huang 2005). Belongia et al. (1999) first demonstrated that, when passing an electrical current through a particle suspension, two distinct solid separation phenomena, namely electrodecantation and electrocoagulation, occurred in a batch reactor. The occurrence of these phenomena strongly depends on the type of the slurry (i.e., predominantly silica or alumina particles) and the conductivity of the suspension. Den and Huang (2005) also demonstrated efficient particle separation by electrocoagulation of dispersed silica particles in a continuous-flow mode, and established the optimum range of operating parameters suitable for treating alkaline CMP wastewater from oxide-film planarization processes.

In these research efforts, much of the focus has been directed

[1]Associate Professor, Dept. of Environmental Science and Engineering, Tunghai Univ., P.O. Box 818, Taichung-Kan Rd., Sec. 3, No. 181, Taichung, Taiwan 407, Republic of China (corresponding author). E-mail: wden@mail.thu.edu.tw

[2]Professor, Graduate Institute of Environmental Engineering, National Chiao Tung Univ., Po-Ai St., No. 75, Hsinchu, Taiwan 300, Republic of China. E-mail: cphuang@mail.nctu.edu.tw

Note. Discussion open until May 1, 2007. Separate discussions must be submitted for individual papers. To extend the closing date by one month, a written request must be filed with the ASCE Managing Editor. The manuscript for this paper was submitted for review and possible publication on April 27, 2005; approved on May 10, 2006. This paper is part of the ***Journal of Environmental Engineering***, Vol. 132, No. 12, December 1, 2006. ©ASCE, ISSN 0733-9372/2006/12-1651–1658/ $25.00.

J. Environ. Eng. 2006.132:1651-1658.

to the experimental evaluation of electrocoagulation for the removal of particles from the liquid medium. The design aspect, in comparison, has not been addressed adequately. In a previous study, Matteson et al. (1995) developed a mathematical model based on electrophoresis and charge neutralization to simulate the kinetics of electrocoagulation process for ultrafine kaolin particles. They found that second-order reaction kinetics could be used to generically describe the particle aggregation and removal processes. Their model, however, was built on the batch-type reactor and extended into a multiple-tank configuration. The primary objective of the present work was to investigate the design basis for a continuous-flow channel reactor, in macroscale transport phenomenon, by using an advection transport model, and to verify the model by both laboratory-scale and pilot-scale studies.

Materials and Methods

CMP Wastewater and Characteristics

The CMP wastewater used throughout this study was obtained from a large-scale semiconductor manufacturing plant in the Science Industrial Park in Hsinchu, Taiwan. The characteristics of the oxide CMP wastewater, which was segregated from other sources of wastewater, somewhat varied depending on the upstream process requirement, but typically contained turbidity in the range between 200 and 600 NTU, conductivity in the range between 50 and 150 μS/cm, and pH in the range between 6.8 and 9.1. The size and distribution of the particles in the CMP wastewater were measured by a Malvern particle analyzer (Mastersizer 2000, Malvern Instruments Ltd., U.K.) with an effective range between 0.01 μm and 2 mm. The electrophoretic mobility of the particles was measured by a zeta (ζ) potential analyzer (ZetaPlus, Brookhaven Instruments Corp., Holtsville, N.Y.) using Doppler shift analysis with laser light scattering. A representative set of the particle size distribution of the raw wastewater, as well as the ζ potential and particle size as a function of wastewater pH, are shown in Fig. 1. The particle size narrowly distributed between 50 and 350 nm, with a geometric mean size of 114 nm. The isoelectric point (IEP) of the wastewater was approximately 2.7, resulting in a mean particle size larger than 2 μm. Furthermore, the particle size appeared to stabilize (≈150 nm) at pH greater than 4, suggesting that particle collision energy was sufficient to overcome the electrical repulsive force for ζ potential less than −20 mV, leading to particle agglomeration and rapid size growth.

In addition to turbidity, the total silica concentration in the wastewater was also analyzed by an inductively coupled plasma–atomic emission spectroscopy (ICP-AES) (Jobin-Yzon JY24, France). The CMP wastewater typically contained total silica concentration between 400 and 800 mg/L, which would correspond to volumetric fraction of 0.4–0.7 to the total solids, assuming a silica density of 2.1 g/mL. Coupled with the observation that the ζ-potential profile for the wastewater was similar to that of pure silica suspension [Fig. 1(b)], it can be inferred that silica was predominant in the CMP wastewater apropos the number of particles, with a part of the turbidity contributed from other particles with much larger size or density. Nevertheless, the silica concentration and turbidity formed a well-behaved linear correlation within the concentration range observed in this study, and thus turbidity was employed as the primary monitoring parameter.

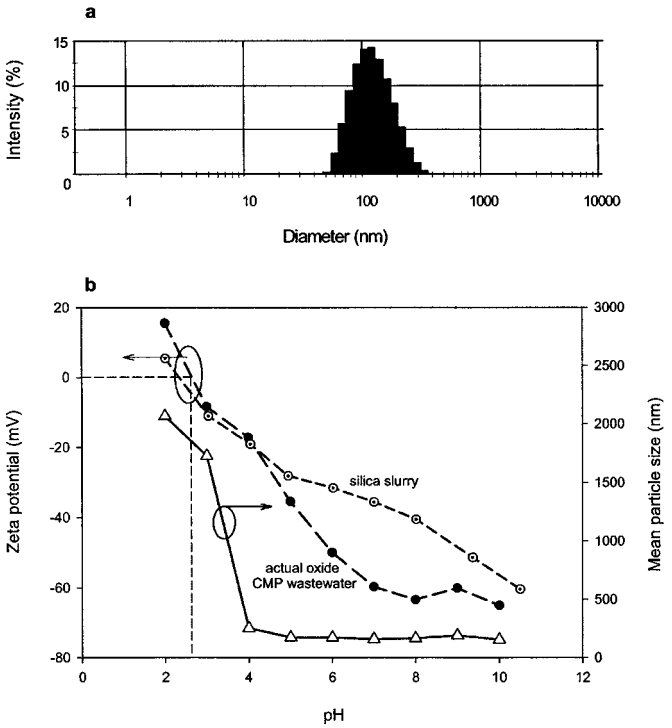

Fig. 1. (a) Particle size distribution of raw CMP wastewater used in this study; (b) variation of zeta-potential (•) and mean particle size (△) as function of initial CMP wastewater pH. Zeta-potential for pure silica slurry is also shown (◦) as comparison.

Experimental Methods

Laboratory-scale (8 L) and pilot-scale (180 L) continuous-flow reactors with similar configuration and dimensional ratios were constructed and operated in the study, as shown schematically in Fig. 2. The reactors of the two scales were geometrically similar with respect to the ratio of length to width to height. Also, the effective area of each electrode plate that channelizes the reactor was 180 mm × 140 mm for the laboratory-scale reactor and 450 mm × 400 mm for the pilot-scale reactor. The anodes (iron plates) were completely submerged, and the cathodes (stainless steel plates) were partially submerged in the suspension. The electrode plates were interposed equidistantly to create vertical flow channels with uniform electrical field strength. The channel width

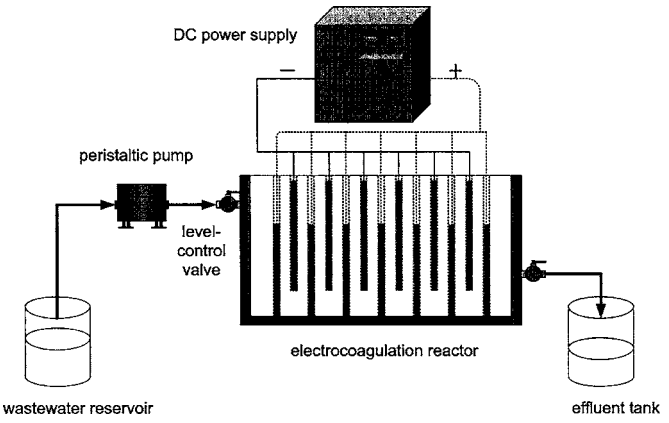

Fig. 2. Experimental apparatus of continuous-flow electrocoagulation system

J. Environ. Eng. 2006.132:1651-1658.

Table 1. Reactor Dimensions and Operating Parameters for Laboratory- and Pilot-Scale Electrocoagulation Studies

Parameter	Laboratory scale	Pilot scale
Reactor interior dimension ($L\times W\times H$) (mm)	$320\times 180\times 200$	$100\times 500\times 600$
Working electrode dimension ($W\times H$) (mm)	180×140	450×400
Working volume (m^3)	8.0×10^{-3}	0.18
Applied current (A)	0.5–2.5	15–25
Volumetric flow rate (m^3/day)	0.12–0.37	1.0–4.0
Hydraulic retention time (min)	30–100	65–260
Number of channels, Min/max	6/14	10/20

can be varied by adding or removing an equal number of electrode plates. Automatic dc power regulators operating in constant-current mode separately supplied the electrical currents to the reactors of different scale. The voltage response was monitored and recorded by a data-acquisition system. The physical dimensions and the range of the operating conditions for both reactors are summarized in Table 1.

At the commencement of each experimental run, the electrocoagulation reactor was filled with the oxide CMP wastewater such that the liquid level was above the anodic plates and below the top of the cathodic plates. Ball valves installed at the effluent end allowed control of steady liquid level in the reactor. The wastewater was continuously pumped from a reservoir into the reactor at various flow rates. Hence, the overall charge loading applied to the wastewater can be calculated using the following expression:

$$\text{charge loading } (C_F) = \frac{i\tau}{FV_r} \tag{1}$$

Therefore, at the full capacity of the operating conditions specified in Table 1, the resulting charge loading ($\sim$20 F/m^3) and current density ($\sim$7 A/m^2) were similar between the reactors of the two scales.

Samples from the influent and effluent ports were taken at a 5-min interval and measured for turbidity, conductivity, and pH by a Hach ratio/XR turbidity meter (Hach Co., Loveland, Colo.). The organic content in the suspensions was measured by a non-dispersive infrared total organic carbon (TOC) analyzer (Shimadzu TOC-5000A, Japan) after samples were filtered with 0.45-μm membrane, acidified, and N_2 purged to remove inorganic carbon. The total residual iron concentration was analyzed by the ICP-AES (Jobin-Yzon JY24, France).

The current efficiency was determined through batch experiments with six pair of electrodes in the laboratory-scale reactor. Instead of CMP wastewater, reversed osmosis (RO) water was used as the electrolyte medium to minimize iron consumption. After 10 min of electrolysis, the electrodes were removed from the reactor, and the aqueous medium was vigorously stirred before samples were taken for total iron analyses with ICP-AES. The current efficiency (ε_c) was defined as the ratio of the actual mass of iron ($[\text{Fe}]_R$) to the theoretical mass of iron ($[\text{Fe}]_T$) liberated from the anodes

$$\varepsilon_c = \frac{[\text{Fe}]_R}{[\text{Fe}]_T} \tag{2}$$

where the theoretical mass of iron liberation is calculated from the Faraday's law for a monopolar system

$$[\text{Fe}]_T = \frac{i\times\tau\times \text{MW}_{\text{Fe}}}{Z\times F} \tag{3}$$

Development of Process Kinetics and Design Approach

The main objective of this study is to determine the process kinetics of electrocoagulation in a continuous-flow reactor with monopolar configuration. For conditions kinetically limited by the rate of particle coagulation, the continuous-flow channels can be essentially viewed as a single parallel-plate channel that follows an axial advection–dispersion model

$$\frac{\partial c}{\partial t} + v\frac{\partial c}{\partial x} = D\frac{\partial^2 c}{\partial x^2} + \Re \tag{4}$$

where $\Re$ represents the reaction kinetics associated with the particle removal due to coagulation. The initial and boundary conditions for the open system are

$$c(x,t=0)=0; \quad c(x=0,t)=c_{in}$$

and

$$D\left.\frac{dc}{dx}\right|_{x=L-} = 0$$

For ultrafine particles, Brownian motion is the primary mechanism for particle interactions, and the coagulation kinetics based on the discrete particle dynamics analysis leads to a second-order reaction $\Re = dc/dt = -kc^2$. Therefore, assuming that the reaction is not limited by the availability of the metal ions (i.e., coagulant) released from the anodes, Eq. (4) can be completed as

$$\frac{\partial c}{\partial t} + v\frac{\partial c}{\partial x} = D\frac{\partial^2 c}{\partial x^2} - kc^2 \tag{5}$$

The particle diffusivity can be estimated by the Stoke–Einstein equation for laminar flow regime

$$D = \frac{k_B T}{3\pi\mu d_p} \tag{6}$$

Since the particle diffusivity is very small ($D\approx 10^{-12}$ m^2/s), the diffusion transport term in Eq. (5) can be neglected. Finally, the equation can be simplified into a first-order ordinary differential equation by assuming steady-state conditions

$$v\frac{\partial c}{\partial x} + kc^2 = 0 \tag{7}$$

whose analytical solution is

$$c(x) = \left(\frac{k}{v}x + \frac{1}{c_0}\right)^{-1} \tag{8}$$

The final equation will be used to determine the actual kinetic constant occurring in the electrocoagulation reactor by best fitting with the experimental values with various operating conditions.

A design approach consisting of experimental evaluation and model simulation was proposed in this study. The design procedure, such as that outlined in Fig. 3, can serve as an effective tool for the a priori evaluation of electrocoagulation process scaleup. Since the model described above excludes the generation of ferrous ions as a rate-limiting factor, the design procedure requires initial experimental evaluation of the operating parameters. In the

J. Environ. Eng. 2006.132:1651-1658.

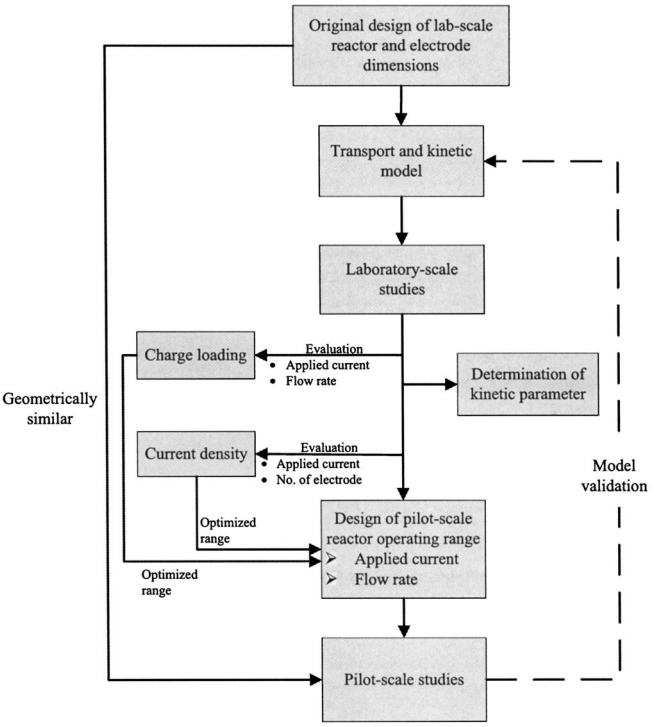

Fig. 3. Design and scale-up procedure for electrocoagulation process

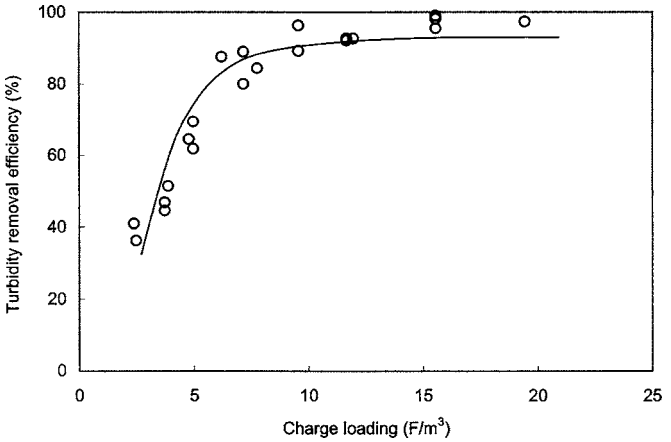

Fig. 4. Effect of charge loading on steady-state turbidity removal efficiency (initial turbidity range =200–400 NTU, pH=8.0–9.2) for laboratory-scale reactor, with characteristic curve represented by solid line

present study, parameter optimization (charge loading and current density) was conducted through a series of rigorous laboratory-scale studies, followed by the experimental determination of coagulation rate constant under the operating conditions established in the previous step. Subsequently, the "optimized" ranges of these parameters from the laboratory-scale studies were applied to the pilot-scale studies. Hence, the range of applied current, wastewater flow rate, and the number of anodes that satisfied the "optimized" criteria could be designed accordingly for the pilot-scale studies.

In this work, the reactors are upscaled such that the dimensions of the reactor interior and the electrodes between the laboratory- and pilot-scale reactors are geometrically similar to eliminate the hydrodynamic variation due to reactor/electrode geometries. Therefore, the design of the pilot-scale operating range, as listed in Table 1, would cover the optimized ranges of charge loading and current density determined from the laboratory-scale studies. Consequently, a series of pilot-scale experiments are performed, and the results are employed to validate the kinetic model.

Results and Discussion

Parameter Optimization with Laboratory-Scale Reactor CMP Wastewater and Characteristics

Effect of Charge Loading

Charge loading is generally considered as a basic technique to evaluate the range of operating conditions necessary to achieve the desired removal efficiency. This surrogate parameter accounts for both hydraulic retention time and the applied current, which theoretically is proportional to the quantity of ferrous ions liberated for electrocoagulation according to the Faraday's law. Fig. 4 shows the effects of charge loading on the steady-state turbidity removal efficiencies for the laboratory-scale experiments. The period of which steady-state conditions (i.e., residual turbidity does not change with time) were typically attained after 60 min of operation. The data clearly clustered into a characteristic profile that indicated a sharp increase in the removal efficiency for charge loadings up to 8 F/m^3, above which the turbidity removal efficiency began to level off. Obviously, under the conditions where low charge loadings were applied to the wastewater, the quantity of ferrous ions as the coagulating agent was insufficient for efficient removal of the silica particles. For charge loadings greater than 8 F/m^3, the turbidity removal was most likely controlled by the rate of particle coagulation and agglomeration, kinetically a much slower process than the colloidal destabilization process. In addition, overdosing of coagulants would lead to particle restabilization and turbidity inversion (i.e., reduced turbidity removal efficiency) due to charge reversal, as commonly experienced during chemical coagulation processes. However, the charge loading curve exhibited in Fig. 3 gives no indication to turbidity inversion even for charge loading as high as 20 F/m^3.

Effects of Current Density

In the electrocoagulation process, the actual current efficiency of the reactor is highly material specific, thereby requiring a basic evaluation prior to its application of particle removal. As shown in Fig. 5, the total iron concentration initially increased with the current density, then stabilized and fluctuated between 3.7 and 5.0 mg/L for current densities greater than 2.8 A/m^2. In general, the current efficiency appeared to be relatively low (<40%) and continually decreased with larger current density to roughly 10%. The low current efficiency was most likely related to surface texture and the impurity contents (e.g., graphite, silicon) in the cast iron anodes (Lescuras-Darrous et al. 2002). The development of a passivating oxide film, which does not easily dissolve in basic solutions, increases the resistivity of the metal and leads to a waste of energy. The underlying metal may become exposed only at localized points owing to some discontinuity in the metal (e.g., defects or grain boundary). However, when a current density was increased to 7.1 A/m^2, the current efficiency as well as the corresponding iron concentration began to increase, suggesting that a critical current density leading to the breakdown of the passivating oxide film may have been reached. While the result of the low

J. Environ. Eng. 2006.132:1651-1658.

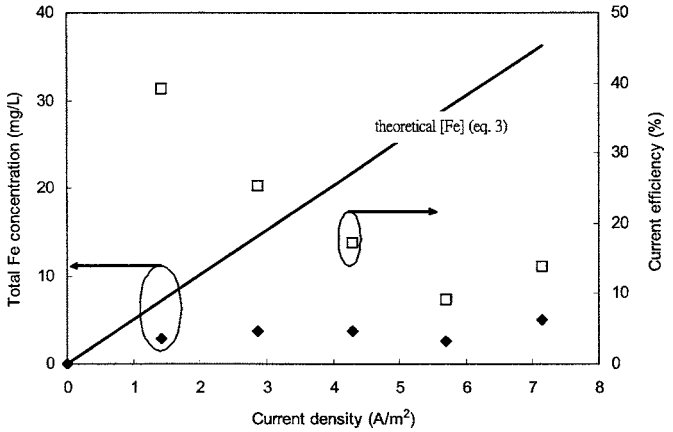

Fig. 5. Total iron concentration actually generated (♦) and theoretically generated (bold solid line) from anodic electrolysis as function of current density (10 min electrolysis in batch runs using reverse osmosis water as background solution with pH 6.9 and conductivity of 24 μS/cm). Corresponding current efficiency is also shown (□).

iron concentration exhibited in Fig. 5 helped explain the absence of overdosing under conditions of high charge loading, the values of actual iron concentration determined from the batch study should not be used to estimate the effluent iron concentration in the continuous-flow studies, nor to serve as a factor for the optimization of the operating parameters.

Although charge loading offers a useful design parameter for the electrocoagulation process, it tends to overlook individual parameters such as the current density and the wastewater retention time. Therefore, evaluation of the effects of these parameters separately is imperative. Figs. 6(a and b) show the effect of current density on the turbidity removal efficiency and the corresponding effluent residual iron concentration, respectively, for the continuous-flow experiments with various hydraulic retention times. When the current density was less than 1.5 A/m^2, none of the experimental runs resulted in turbidity removal efficiency over 50%, while the corresponding residual iron concentration remained very low. These results imply that silica removal was mainly limited by the availability of ferrous ions released from the anodic surfaces. As the current density was increased, the turbidity removal efficiencies for all retention times were invariably enhanced due to the greater quantity of iron dissolution. One should note that the accelerated particle migration toward anodic surfaces due to the stronger electrical field at a greater applied current is not considered as an important factor, because the particle migration time was at least two orders of magnitude smaller than the hydraulic retention times experimented in this study. In particular, Fig. 6(a) shows that the turbidity removal efficiency for the retention time of 30 min increased rather slowly with the current density up to 4.3 A/m^2, then accelerated at larger current densities. Incidentally, as shown in Fig. 6(b), the effluent residual iron concentration for $\tau=30$ min increased sharply with current density exceeding 2.9 A/m^2, peaking at 4.5 A/m^2. The accumulation of the total iron concentration suggested that the process was initially controlled by the rate of coagulation rather than the availability of ferrous ions. However, the subsequent reduction of the residual iron concentration with larger current densities entailed other mechanisms that enhanced the consumption (i.e., particle coagulation) of ferrous ions. Among other possibilities, the improved mixing (e.g., bubble production, fluid regime, particle

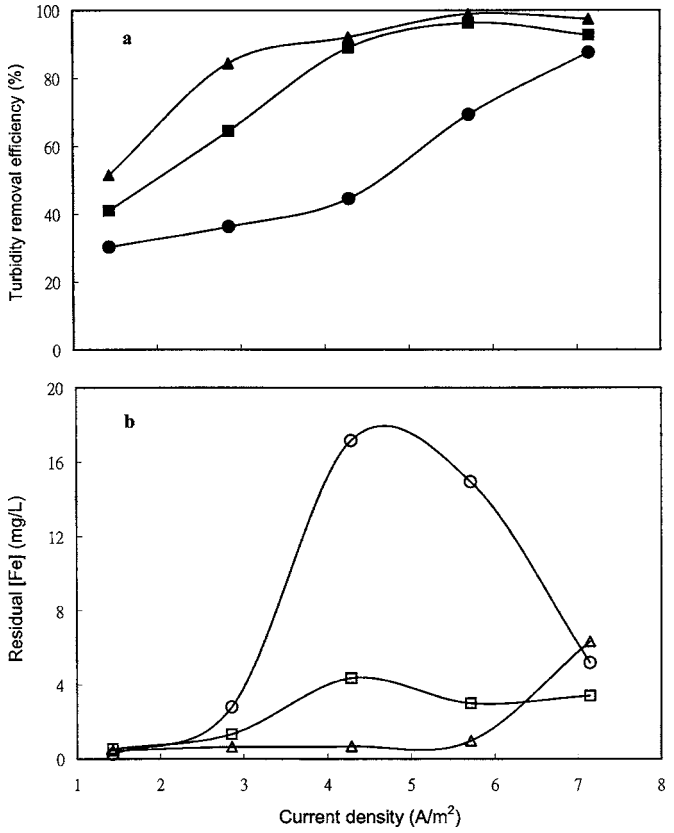

Fig. 6. Dependence of: (a) steady-state turbidity removal efficiency; (b) effluent residual iron concentration as function of current density [(•, ◦) $\tau=30$ min; (■, □) $\tau=60$ min; (▲, △) $\tau=100$ min]

migration velocity) within each cell as a result of greater current density was considered as the primary cause. On the contrary, the turbidity removal efficiencies for the longer retention times (60 and100 min) exhibited similar patterns, both increasing drastically before leveling off, or even slightly decreasing, at larger values of current density. The corresponding residual iron concentration profiles also demonstrated the accumulation of coagulants at larger current densities, however the extents of their accumulations were much less than that for $\tau=30$ min. In principle, the quantity of residual iron concentration for all experimental runs strongly reflected the turbidity removal efficiency.

Effects of Initial Wastewater pH

As in any other treatment processes, the effects of wastewater pH on the process performance must be evaluated. During electrocoagulation processes, the effects of wastewater pH are principally twofold, namely the degree of surface charges and the speciation of coagulant formed under the pH. For iron anodes, ferrous ion [i.e., Fe(II)] is the common in situ product of iron electrolysis. Fe(II) can be easily oxidized into Fe(III) in the particulate form of $Fe(OH)_3$, especially under neutral or weak alkaline conditions. Oxygen and hydrogen gases are evolved at the anodic and cathodic sides, respectively, to complete the redox reactions

Anode

$$Fe \rightarrow Fe^{2+} + 2e^- \tag{9a}$$

$$4Fe^{2+}_{(aq)} + O_{2(aq)} + 10H_2O \rightarrow 4Fe(OH)_{3(s)} + 8H^+_{(aq)} \tag{9b}$$

J. Environ. Eng. 2006.132:1651-1658.

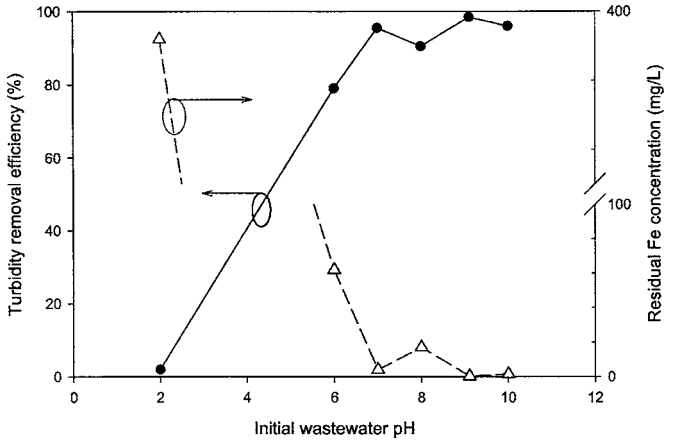

Fig. 7. Effects of initial wastewater pH on steady-state turbidity removal efficiency and corresponding residual iron concentration (j=5.7 A/m^2; τ=100 min)

$$2H_2O \rightarrow O_{2(g)} + 4e^- + 4H^+_{(aq)} \quad (9c)$$

Cathode

$$2H_2O + 2e^- \rightarrow 2OH^- + H_{2(g)} \quad (10)$$

Fig. 7 shows the variation of the turbidity removal efficiency and the corresponding residual iron concentration with the initial wastewater pH under identical current density and retention time. As seen previously, the residual iron concentration formed a mirror image of the turbidity removal efficiency. Under strong acidic condition (pH 2), no discernible turbidity removal was observed, a result attributed to the near IEP where silica particles essentially contained no surface charge, thereby minimizing the possibility of particle migration and charge neutralization with the ferrous ions. For pH above 6, the turbidity removal efficiency generally exceeded 80% with considerably less residual iron concentrations, indicating surface charge was no longer the limiting factor. It is interesting to note, however, that the turbidity removal was less efficient at pH 6 than those above pH 7, even though the primary hydrolytic species are positively charged [e.g., $Fe(OH)^+_2$, $Fe(OH)^{2+}$] under weak acidic conditions as opposed to the negatively charged species [e.g., $Fe(OH)_4$] under alkaline conditions. Hence, the ferrous ions, rather than its hydrolytic species, appeared to be the primary coagulating agent binding to the silica colloids near the surface of the anodes. Based on these results, no pH adjustment was needed for the oxide CMP wastewater, which typically had a pH ranging between 8 and 9. Furthermore, for wastewater with initial pH$\geq$6, the final effluent pH all increased toward a range of 10.5–11.2, suggesting that the hydrogen evolution reaction [Eq. (10)] at the cathodes was dominant over the H^+ generating reactions [Eqs. (9b) and (9c)]. The intense hydrogen gas evolution also partially reflects the low current efficiency as manifested in Fig. 4.

Determination of Reaction Kinetic Constant

The results of parameter optimization, as shown in Fig. 6, suggest the turbidity removal efficiencies above 90% with low residual iron concentrations were attained when the current density was greater than 5.7 A/m^2 and the retention time longer than 60 min. These operating conditions corresponded to charge loadings greater than 9.6 F/m^3. Consequently, by eliminating the availability of Fe(II) as the limiting factor, these parameters were selected as the minimum criteria for the evaluation of reaction (coagulation) kinetic parameter. By linearization of Eq. (8) into Eq. (11), the kinetic constant can then be estimated from the slopes of the linearized relationship between the steady-state concentration and the channel position

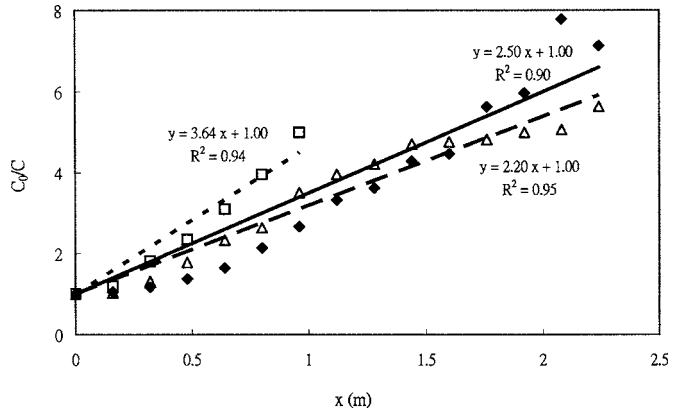

Fig. 8. Determination of second-order rate constant by Eq. (11) with data points and regression lines [(△) C_F=9.6 F/m^3; ν=6.0 $\times 10^{-2}$ m/s; (◆) C_F=15.5 F/m^3; ν=3.7$\times 10^{-2}$ m/s; (□) C_F=9.6 F/m^3; ν=2.4$\times 10^{-2}$ m/s; initial turbidity between 85 and 400 NTU]

$$\frac{c_0}{c} = \frac{kc_0}{\nu}x + 1 \quad (11)$$

Fig. 8 shows the experimental data profiles and the corresponding linear regression curves obtained from the laboratory-scale studies under three different sets of operating conditions (i.e., average flow velocity, number of channels, initial turbidity) that meet the aforementioned criteria. Since the initial number concentration of silica particles (between 0.5×10^{18} and 1.5×10^{18} L/m^3) and flow velocity are known values, the kinetic constant (k) could be easily determined from the slope (kc_0/ν) of each linear regression curve. As a result, the average second-order rate constant was 1.2×10^{-21} m^3/s. One should note that the fast coagulation of submicrometer particles with similar size category theoretically follows the Brownian coagulation kinetics, whose rate constant is determined by the collision frequency function to give $k=4k_BT/3\mu$. This calculation results in a k value on the order of 10^{-18} m^3/s, which would have significantly overestimated the actual rate of coagulation for this particular electrocoagulation process. It has been documented that the size differential between the coagulating colloids may reduce the collision efficiency by interaction energy barrier or other hydrodynamic interactions unaccounted in the case of fast coagulation theory (Han and Lawler 1992). Therefore, experimental determination of the kinetic parameter is deemed necessary for the design of electrocoagulation reactors, particularly for those involving treatment of aqueous suspensions containing unknown particulate components.

Pilot-Scale Verification and Simulation

Pilot-scale electrocoagulation studies were conducted to evaluate the turbidity removal efficiency for the on-site oxide CMP wastewater, and to validate the kinetic model described in Eq. (4). The pilot-scale reactor was subjected to different operating conditions

J. Environ. Eng. 2006.132:1651-1658.

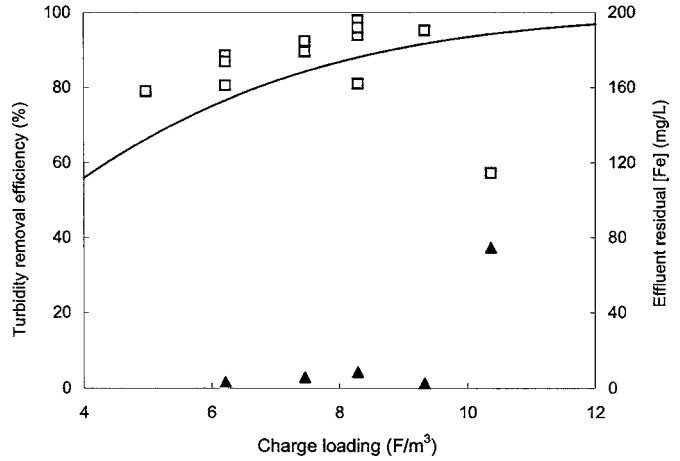

Fig. 9. Effect of charge loading on steady-state turbidity removal efficiency (initial turbidity between 200 and 400 NTU) and residual iron concentration (▲) for pilot-scale experiments. Characteristic curve obtained from Fig. 3 (laboratory-scale data) is superimposed for comparison.

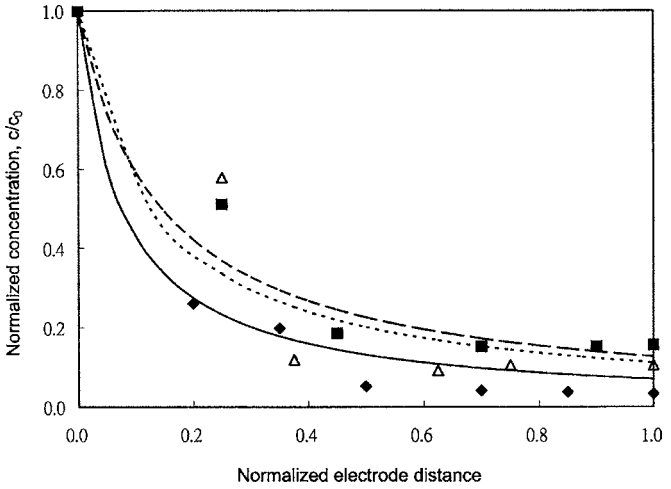

Fig. 10. Experimental data (symbols) and model profiles (lines) of normalized concentrations as function of normalized distance for various pilot-scale conditions [(◆;–) C_F=8.3 F/m^3; ν=1.7 $\times 10^{-2}$ m/s, 20 channels; (■,—) C_F=6.3 F/m^3; ν=2.3$\times 10^{-2}$ m/s, 20 channels; (△,···) C_F=8.3 F/m^3; ν=8.7$\times 10^{-3}$ m/s, 12 channels; initial turbidity between 420 and 500 NTU]

specified in Table 1. The range of operating conditions yielded charge loading between 5.0 and 10.4 F/m^3 and current density between 4.4 and 7.3 A/m^2.

Fig. 9 shows the effects of charge loading in the pilot-scale study on the turbidity removal efficiency and the corresponding residual iron concentrations, along with a portion of the characteristic curve presented in Fig. 4 for the laboratory-scale studies. As one can observe from Fig. 9, the results from the pilot-scale study generally conformed to those from the laboratory-scale study, requiring a charge loading greater than about 8 F/m^3 to attain turbidity removal efficiency exceeding 90%. An exception occurred at the charge loading of 10.4 F/m^3 under which less than 60% efficiency was observed. For this particular data point, the operating current density was approximately 14 A/m^2 (i=25 A with 10 channels), which was well beyond the range of current density tested during the laboratory-scale experiments. As a result, the effluent appeared severely greenish due to the accumulation of ferrous ions, which likely contributed to the increase in the effluent turbidity. Therefore, the applied current was kept well below this value for the ensuing pilot-scale model validation studies.

The experimental data and the model profiles for three pilot-scale runs with different operating conditions, including the number of flow channels (with identical reactor working volume) and wastewater flow rates, are presented in Fig. 10. The position (i.e., the cell number) where samples were collected was treated as the corresponding length of anodic surface by which the wastewater had passed, thereby assuming electrocoagulation was active for all parts along the height of each anodic plate. One can readily observe that the trend of the data profile for each experimental condition was correctly depicted by the model simulation, although the local discrepancies between the experimental and model profiles were significant near the entrance portion of the reactor. A part of these discrepancies could be ascribed to the fact that electrocoagulation is active only in the overlapping region between each pair of electrodes, as the opening at each turn of cell forms an incomplete flow channel. Nevertheless, the discrepancy tended to diminish toward the latter parts of the reactor.

The model was further validated by a series of pilot-scale experiments using different number of anodes (and thus flow channels) with identical interelectrode gap, resulting in varying reactor working volume proportional to the number of channels. Fig. 11 illustrates the turbidity removal efficiency of the effluent as a function of the number of flow channels, again expressed as the total length of anodic surface available for electrocoagulation. With the supply of a constant current (i=20 A), these operating conditions represented charge loading of 8.3 F/m^3 and current density ranging between 5.6 and 11 A/m^2. Evidently, the model profile agreed reasonably well with the experimental data, although the predicted removal efficiencies for less than ten channels (denoted with dashed line) were not verified experimentally. In summary, these validation studies manifested the suitability of the kinetic transport model for the design of the channel-flow electrocoagulation process. One should also note that, although

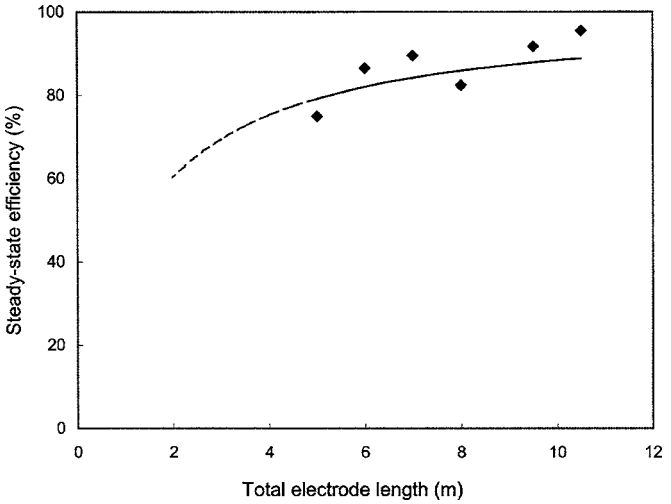

Fig. 11. Steady-state turbidity removal efficiency (◆) and model simulation profile (—) for pilot-scale runs with various numbers of anode (i=20 A; $C_F \geq$8.3 F/m^3; ν=1.7$\times 10^{-2}$ m/s; initial turbidity between 380 and 490 NTU)

J. Environ. Eng. 2006.132:1651-1658.

the kinetic relationships derived from the transport-reaction equations were verified using the fixed electrode configuration in the present work, they would remain applicable for different ele-trode geometries insofar as parallel-plate channels with similar hydrodynamic behavior of the bulk flow [e.g., sufficient width (W) and height (H)] are formed. However, electrocoagulation with reactor or electrode geometries significantly different from the ones used here (e.g., concentric cylinders, packed bed) is beyond the scope of this study.

Conclusions

Meager information is available on the systematic approach for the design of electrocoagulation processes, probably because the process is highly case-specific as the electrode materials, the electrical configurations, and the wastewater properties all play an immense role to the effectiveness of the system. Determination of the kinetic constant in the electrocoagulation process, hence, is an important step toward the proper reactor design of larger scales. This process entails the establishment of the operating criteria ensuring that the electrocoagulation process is controlled by the rate of coagulation rather than the availability of the metal ions. For a system consisting of a continuous-flow channelized reactor with a monopolar (iron anodes) scheme to treat an alkaline CMP wastewater containing dispersed ultrafine silica particles, the criteria of the operating parameters to guarantee such conditions include charge loading $\geqslant 8\ \mathrm{F/m^3}$, current density $\geqslant 5.7\ \mathrm{A/m^2}$, and retention time $\geqslant 60$ min. pH does not play an important role in the system performance as long as the wastewater remains alkaline. High turbidity removal efficiency ($>90\%$) and low residual iron concentration in the effluent can be attained under these operating conditions. Excessively high current density, however, causes system performance deterioration due to the accumulation of ferrous ions.

Simplifications from the fundamental axial advection–dispersion equation with second-order reaction kinetics lead to a linear expression suitable for the determination of the kinetic constant. A series of laboratory-scale experiments under coagulation-limiting conditions yield an average second-order constant of $1.2\times10^{-21}\ \mathrm{m^3/s}$ for silica particle concentration between 0.5×10^{18} and $1.5\times10^{18}\ \mathrm{L/m^3}$. This value is approximately three orders of magnitude smaller than the Brownian coagulation rate constant. The model was further validated by the pilot-scale electrocoagulation studies performed under the required operating conditions, justifying the simplification of the channelized-flow configuration into a long parallel-plate channel. Therefore, the simplistic model and the kinetic constant can be used as a preliminary design and scaling basis for the monopolar continuous-flow electrocoagulation reactor.

Acknowledgments

The writers are grateful for the financial support from the Winbond Electronics Corp., and the experimental assistance by Mr. P.-T. Lin and Mr. H.-C. Ke of the Graduate Institute of Environmental Engineering at the National Chiao Tung University.

Notation

The following symbols are used in this paper:

- C = particle number concentration ($\mathrm{L/m^3}$);
- C_F = charge loading ($\mathrm{F/m^3}$);
- c_0 = initial particle number concentration ($\mathrm{L/m^3}$);
- D = colloidal diffusivity ($\mathrm{m^2/s}$);
- d_p = mean particle diameter (m);
- F = Faraday constant (96,500°C);
- i = current input (A);
- j = current density ($\mathrm{A/m^2}$);
- k = second-order kinetic constant ($\mathrm{m^3/s}$);
- k_B = Boltzmann constant (1.38×10^{-23} J/K);
- $\mathrm{MW_{Fe}}$ = molecular weight of iron (g/mol);
- T = temperature (K);
- V_r = reactor volume ($\mathrm{m^3}$);
- x = axial distance along length of anode plates (m);
- Z = metal ion valence (=2 for ferrous ions);
- ε_c = current efficiency (%);
- μ = fluid viscosity (kg/m s);
- ν = wastewater flow velocity (m/s); and
- τ = hydraulic retention time (min).

References

Belongia, B. M., Haworth, P. D., Baygents, J. C., and Raghavan, S. (1999). "Treatment of alumina and silica chemical mechanical polishing waste by electrodecantation and electrocoagulation." *J. Electrochem. Soc.*, 146(11), 4124–4130.

Chen, G., Chen, X., and Yue, P. L. (2000). "Electrocoagulation and electroflotation of restaurant wastewater." *J. Environ. Eng.*, 126(9), 858–863.

Den, W., and Huang, C. (2005). "Electrocoagulation for removal of silica nanoparticles from chemical-mechanical planarization wastewater." *Colloids Surf., A*, 254(2), 81–89.

Dobolyi, E. (1978). "Experiments aimed at the removal of phosphate by electrochemical methods." *Water Res.*, 12(12), 1113–1119.

Ge, J., Qu, J., Lei, P., and Liu, H. (2004). "New bipolar electrocoagulation-electroflotation process for the treatment of laundry wastewater." *Sep. Purif. Technol.*, 36(1), 33–39.

Golden, J. H., Small, R., Pagan, L., Chang, C., and Ragavan, S. (2000). "Evaluating and treating CMP wastewater." *Semicond. Int.*, 23(11), 85–98.

Han, M., and Lawler, D. F. (1992)."The relative insignificance of G in flocculation." *J. Am. Water Works Assoc.*, 84(10), 79–91.

Holt, P. K., Barton, G. W., Wark, M., and Mitchell, C. A. (2002). "A quantitative comparison between chemical dosing and electrocoagulation." *Colloids Surf., A*, 211(2–3), 233–248.

Lai, C. L., and Lin, S. H. (2003). "Electrocoagulation of chemical mechanical polishing (CMP) wastewater from semiconductor fabrication." *Chem. Eng. J.*, 95(1), 205–211.

Lescuras-Darrous, V., Lapicque, F., and Valentin, G. (2002). "Electrochemical ferrate generation of waste water treatment using cast irons with high silica contents." *J. Appl. Electrochem.*, 32(1), 57–63.

Lin, S. H., and Chi, F. P. (1994). "Treatment of textile wastewater by electrochemical methods." *Water Res.*, 28(2), 277–282.

Matteson, M. J., Dobson, R. L., Glenn, R. W., Kukunoor, N. S., Waits, W. H., and Clayfield, E. J. (1995). "Electrocoagulation and separation of aqueous suspensions of ultrafine particles." *Colloids Surf., A*, 104(1), 101–109.

Tsouris, C., DePaoli, D. W., Shor, J. T., Hu, Z.-C., and Ying, T.-Y. (2001). "Electrocoagulation for magnetic seeding of colloidal particles." *Colloids Surf., A*, 177(2–3), 223–233.

J. Environ. Eng. 2006.132:1651-1658.